JOURNAL OF GEOPHYSICAL RESEARCH, VOL. 101, NO. B5, PAGES 11,565–11,577, MAY 10, 1996

Modeling gravity-driven flows on an inclined plane

Barbara C. Bruno
Department of Earth Sciences, The Open University, Milton Keynes, England

Stephen M. Baloga
Proxemy Research Incorportated, Laytonsville, Maryland

G. Jeffrey Taylor
Hawaii Institute of Geophysics and Planetology, University of Hawaii at Manoa, Honolulu, Hawaii

Abstract. We develop an exact analytic solution for unconfined flows having an assumed rheology advancing on an inclined plane. We consider the time-dependent flow movement to be driven by gravitational transport and hydrostatic pressure. We examine how these two forces drive flow movement in the downstream and cross-stream directions by adopting a volume conservation approach. Simplifying assumptions reduce the governing equation to the dimensionless form $\partial/\partial x(\alpha h^m) = \partial/\partial y(\alpha h^m \partial h/\partial y)$, where x and y are the downstream and cross-stream directions, respectively; h is the flow depth; and $\alpha = \alpha(x)$ and m are prescribed by the rheology of the fluid. We solve this equation analytically for flows of arbitrary m and α using a similarity transformation. This method involves transforming variables and reducing the governing equation to a nonlinear ordinary differential equation. Our solution determines how flow depth and width change with distance from the source of the flow for different α and m based on known or assumed initial parameters. Consequently, from the traditional geometric dimensions of the deposits, these rheological parameters can be inferred. We have applied the model to basaltic lava flows and found m values typically between 1 and 2. This contrasts with Newtonian fluids, for which m=3. The model of $\alpha(x)$ corresponding to constant viscosity approximates the field data of pahoehoe toes (<5 meters in length), whereas models of $\alpha(x)$ corresponding to linearly increasing and exponentially increasing viscosities better approximate the remote sensing data of longer flows (several kilometers in length).

Introduction

Bruno et al. [1992, 1994] developed a technique to glean information regarding flow emplacement and rheology from the fractal properties of lava flow margins. We found that as frozen snapshots of the final moments of flow, plan view shapes hold important information regarding lava flow dynamics and rheology. In this work, we again exploit the final shape of a lava flow as a source of rheological information, using an altogether different method. We model downstream changes in flow depth and width for flows of different rheological characteristics, and then apply this model "backward" to infer or constrain these rheological characteristics given depth and width profiles. We note that this model can also be applied to other types of unconfined geologic deposits, such as volcanic lahars and mud flows.

A critical assumption of the formulation of the problem is that the volumetric flow rate in the downstream direction represents a conserved quantity. The conservation of volume for an unconfined flow of depth $h = h(x, y, t)$ on an inclined plane is described by

$$\frac{\partial h}{\partial t} + \vec{\nabla}\vec{q} = 0 \tag{1a}$$

where

$$\vec{\nabla} = \frac{\partial}{\partial x}\vec{i} + \frac{\partial}{\partial y}\vec{j} \tag{1b}$$

and where t is time; q is the volumetric flow rate per unit width; and x and y are the spatial coordinates in the downstream and cross-stream directions, respectively. (All mathematical symbols are summarized in the notation section.) Equation (1a) is a form of the first-order conservation equation relating flow of a given variable (i.e., h) to its time rate of change. Solutions to these equations are called kinematic waves [e.g., *Lighthill and Whitham*, 1955; *Baloga*, 1987]. Applying kinematic wave theory to volcanic lahars and considering only the downstream (x) direction, *Weir* [1982] considered solutions to (1a) of the form

$$q = bf(\theta)h^m \tag{2}$$

where b and m are constants and $f(\theta)$ is some function of surface slope. As noted by *Weir* [1982], many different types of transport processes have been modeled with a flow rate of the form shown in (2) featuring a power law relationship between flow rate (q) and flow depth (h), a spatially dependent prefactor β (which in (2) depends on a

Paper number 96JB00178.
0148-0227/96/96JB-00178$09.00

constant b and the surface slope θ) and a positive constant m. The empirically determined m values of 3/2 and 5/3 give the Chezy and Manning laws, respectively, for rivers with β dependent on the square root of the slope. The Shamov law is given by m=7/6 with β independent of slope, whereas the Sribniy law is given by m=5/3 with β dependent on the fourth root of slope. Both the Shamov and Sribniy laws have been used to describe transport of mud flows [*Gol'din and Lyubashevskiy*, 1966]. In quantifying the risk from volcanic lahars, *Weir* [1982] obtained m values in the range 1.2-2.0 with a β dependence on the underlying slope similar to that of empirical river laws. Other diverse applications based on a flow rate of the form of (2) include rainfall runoff [*Sherman*, 1978], channel flow with infiltration [*Sherman*, 1981], laminar flow of glaciers [*Paterson*, 1969, chapter 6], surface irrigation [*Sherman and Singh*, 1978], and dam bursting [*Hunt*, 1982]; see *Weir* [1982, 1983] for a thorough review of the literature. The classic treatment of such flow rate forms derives from the problem of river flooding [*Lighthill and Whitham*, 1955] with other notable early papers addressing the response of glaciers to various environmental factors [e.g., *Nye*, 1960, 1963].

In this work, we explore the relevance of a flow rate of the form of (2) in describing transport of lava flows of arbitrary rheology. Our approach is to generalize the volumetric flow rate per unit width of Newtonian fluids given by

$$\vec{q} = -\frac{g}{3\nu}\cos\theta h^3 \vec{\nabla} h + \frac{g}{3\nu}\sin\theta h^3 \vec{i} \tag{3}$$

to include *Weir*'s [1982] relation (equation (2)). Thus we adopt the generalized flow rate

$$\vec{q} = -\alpha g\cos\theta h^m \vec{\nabla} h + \alpha g\sin\theta h^m \vec{i} \tag{4}$$

where $\alpha=\alpha(x)$ and m, a positive constant, are prescribed by the rheology of the fluid. Our approach is to solve the volume conservation equation (equation (1a)) using the flow rate given in (4) and to compare the theoretical solution with data. If the solution describes the data, we shall conclude the assumed flow rate is a reasonable model for lava flows; otherwise, we will conclude that the assumed flow rate is not appropriate. We note that (4) does not account for instabilities (e.g., due to surface tension); the possible development of instabilities in viscous fluids has been addressed in the literature [*Huppert*, 1982a, b; *Lister*, 1992].

Equation (4) incorporates *Weir*'s [1982] power law dependence on flow depth and an arbitrary spatially dependent change in the rheological parameter α. We note that this assumed power law relationship is unrelated to the power law relationship between shear stress and strain rate (i.e., "power law rheology") that characterizes certain fluids. Like (2), equation (4) expresses the influence of gravity in the downstream (x) direction and the influence of hydrostatic pressure according to the gradient of the depth of the flow. For Newtonian fluids of constant viscosity (m=3 and $\alpha=1/3\nu$, where ν is kinematic viscosity), equation (4) reduces to (2). *Smith* [1973] found an analytical solution for this special case [see also *Lister*, 1992]. For non-Newtonian flows, the parameter m may be greater or less than 3 and can be empirically determined by comparing our solution to (4) with flow shape. If, for example, the associated flow depth for a non-Newtonian fluid is less than the Newtonian equivalent for a given flow rate, then it follows that $m > 3$.

For flows of nonconstant viscosity, the parameter α is free to vary spatially. However, this spatial dependence is permitted only in the downstream direction; any cross-stream variations in viscosity are assumed to be small in comparison with changes in the downstream direction. Like m, $\alpha(0)$ is a positive constant.

Smith [1973] showed that substituting the flow rate for a Newtonian fluid (equation (2)) into the volume conservation law (equation (1a)) generates a differential equation having the form of the nonlinear diffusion equation under certain restrictions and simplifications with free boundaries on the surface of the flow. Obtaining this differential equation requires that gravity is the predominant influence on the downstream motion (i.e., the influence of the hydrostatic pressure gradient in the downstream direction is relatively small), while the concomitant lateral expansion of the flow is due solely to hydrostatic pressure. In the steady state, *Smith* [1973] found a remarkable similarity solution that matches the free-boundary condition for the lateral expansion of the flow as a function of distance from the source.

In this paper, we generalize the volumetric flow rate used by *Smith* [1973] to embrace *Weir*'s [1982] relation and an arbitrary spatially dependent change in the flow viscosity. To solve the resulting nonlinear diffusion equation for volume conservation, we show that there exists a transformation of the differential equation into the original *Smith* [1973] form and obtain corresponding solutions for different types of rheologies. As required by the case of a Newtonian fluid of constant viscosity [*Smith*, 1973], the generalized case requires both that gravity is the predominant influence on the downstream motion and the accompanying widening of the flow downstream is due solely to hydrostatic pressure.

Steady State Similarity Solution

The solution described in this section applies to the steady state, i.e.,

$$\vec{\nabla}\vec{q} = 0. \tag{5}$$

The steady state (or time-independent) solution is presumably the asymptotic form of physically reasonable time-dependent solutions. At the source of the flow, we have the boundary conditions

$$h\,(x = 0,\, y = 0) = h_0 \tag{6a}$$

$$h\,(x = 0,\, y = \pm w_0) = 0 \tag{6b}$$

where h_0 and w_0 are prescribed positive constants which represent the depth and half width of the flow, respectively, at the source. Because the flow margin is a free boundary and can expand according to the local dynamics, we must also find the function $w=w(x,t)$ such that for all $t \geq 0$,

$$h\,(x\,, y = \pm w) = 0 \tag{6c}$$

that is, the flow has a finite width. We do not require that a comparable boundary condition be satisfied in the downstream direction, thus allowing the flow to have infinite length.

To obtain an exact analytic solution in the steady state, we convert the steady state partial differential equation and supplementary conditions to dimensionless form using the following substitutions:

$$h = h_0 h^* \tag{7a}$$

$$x = L x^* \tag{7b}$$

$$y = w_0 y^* \tag{7c}$$

$$w = w_0 w^* \tag{7d}$$

$$\alpha = \alpha_0 \alpha^* \tag{7e}$$

where asterisked parameters are dimensionless and the downstream length scale (L) is yet to be determined. Unlike the other scaling factors (h_0, w_0 and α_0), the parameter L does not represent a condition at the source nor is it constrained by flow dimensions; it is a free parameter.

Combining (4), (5), and (7) results in the dimensionless partial differential equation

$$\frac{\partial}{\partial y^*}\left(\alpha^* h^{*m}\frac{\partial h^*}{\partial y^*}\right)+\left(\frac{w_0}{L}\right)^2\frac{\partial}{\partial x^*}\left(\alpha^* h^{*m}\frac{\partial h^*}{\partial x^*}\right) = \left(\frac{\sin\theta w_0^2}{\cos\theta L h_0}\right)\frac{\partial}{\partial x^*}\left(\alpha^* h^{*m}\right) \tag{8a}$$

or, dropping asterisks to simplify notation (but remembering all terms are dimensionless),

$$\frac{\partial}{\partial y}\left(\alpha h^m\frac{\partial h}{\partial y}\right)+\left(\frac{w_0}{L}\right)^2\frac{\partial}{\partial x}\left(\alpha h^m\frac{\partial h}{\partial x}\right)=\left(\frac{\sin\theta w_0^2}{\cos\theta L h_0}\right)\frac{\partial}{\partial x}\left(\alpha h^m\right). \tag{8b}$$

The corresponding dimensionless form of the supplementary conditions is given by

$$h\,(x=0,\,y=0)=1 \tag{9a}$$

$$h\,(x=0,\,y=\pm 1)=0 \tag{9b}$$

$$h\,(x,\,y=\pm w(x))=0 \tag{9c}$$

$$\partial h/\partial y\,(x,\,y=0)=0 \tag{9d}$$

$$w(0)=1 \tag{9e}$$

$$\alpha(0)=1. \tag{9f}$$

In the interest of simplifying (8b), we define the length scale

$$L=\frac{w_0^2}{h_0}\tan\theta. \tag{10a}$$

Furthermore, we require that the influence of the hydrostatic pressure in the downstream direction is small compared to the direct gravitational transport of fluid elements and the cross-stream influence of hydrostatic pressure such that

$$\left(\frac{w_0}{L}\right)^2\frac{\partial}{\partial x}\left(\alpha h^m\frac{\partial h}{\partial x}\right)\ll 1 \tag{10b}$$

and can therefore be disregarded. The partial differential equation (8b) can then be written in the form

$$\frac{\partial}{\partial x}\left(\alpha h^m\right)=\frac{\partial}{\partial y}\left(\alpha h^m\frac{\partial h}{\partial y}\right). \tag{11}$$

When the geometric considerations for a flow indicate that (10b) is satisfied, solutions to (11) describe how flow depth changes, both downstream and laterally. We will then be able to solve for the unknown function $w=w(x)$, which describes how flow width changes downstream.

Smith [1973] solved (11) analytically for a Newtonian fluid (i.e., $m=3$ and $\alpha(x)=1/3\nu$, where ν is kinematic viscosity) with a constant viscosity using the method of similarity transformation. Our approach requires transformation of (11) to the form obtained by Smith, but our subsequent analysis highlights some important differences for the dynamics of the problem.

We begin our approach by transforming away the dependence on the arbitrary function $\alpha(x)$ in the governing (11). This function characterizes the spatially dependent resistance to flow caused by viscosity, surface friction, and any other forces. Here, we rid our equation of $\alpha(x)$, leaving a transformed equation that can be more readily solved by similarity methods, even though the arbitrary function remains embedded in the dependent and independent variables. Instead of a differential equation for h, we transform the partial differential equation to one that applies to a related variable ξ defined by

$$h(x,y)=\alpha(x)^{-1/m}\xi(x,y). \tag{12}$$

Instead of the independent variable x, we use a related variable z:

$$z=\int_0^x\frac{dx'}{\alpha(x')^{1/m}}. \tag{13}$$

With these new variables, (11) becomes

$$\frac{\partial}{\partial z}\left(\xi^m\right)=\frac{\partial}{\partial y}\left(\xi^m\frac{\partial\xi}{\partial y}\right). \tag{14a}$$

Explicitly differentiating (14a) yields the equivalent expression

$$\frac{\partial\xi}{\partial z}=\frac{\xi}{m}\frac{\partial^2\xi}{\partial y^2}+\left(\frac{\partial\xi}{\partial y}\right)^2. \tag{14b}$$

Equation (14b) is a partial differential equation with one dependent variable (ξ) and two independent variables (y,z). It is a transformed version of (11) which also has one dependent variable (h) and two independent variables (x,y). We now apply a similarity construct for the purpose of transforming (14b) into an ordinary differential equation with one dependent variable (G) and one independent variable (η). Following *Smith* [1973], we introduce the similarity construct

$$\xi(\eta,z)=(1+az)^r\,G(\eta) \tag{15}$$

with

$$\eta=y(1+az)^q \tag{16}$$

where a, r, and q are positive constants to be determined.

This construct will constitute a similarity solution provided (1) the constants a, r, and q can be determined; (2) the partial differential equation (14b) reduces to an ordinary differential equation; and (3) the resulting ordinary differential equation has a solution that satisfies boundary conditions corresponding to those appearing in (9).

With the transformations shown in (15) and (16), the supplementary conditions shown in (9) translate to

$$G(0) = 1 \tag{17a}$$

$$G'(0) = 0 \tag{17b}$$

$$G(\pm 1) = 0 \tag{17c}$$

The reader may check, by explicitly differentiating (15), that

$$\frac{\partial \xi}{\partial z} = a(1+az)^{r-1}\left[rG + q\eta G'\right] \tag{18a}$$

$$\frac{\partial \xi}{\partial y} = (1+az)^{r+q} G' \tag{18b}$$

$$\frac{\partial^2 \xi}{\partial^2 y} = (1+az)^{r+2q} G'' \tag{18c}$$

Substituting the expressions of (18) into (14b) yields

$$a(1+az)^{r-1}\left[rG + q\eta G'\right] = (1+az)^{2r+2q}\left[\frac{GG''}{m} + G'^2\right]. \tag{19}$$

Note that the factor $(1+az)$ appears on each side of (19) with different exponents. By definition, similarity transformations are absolutely invariant; they necessarily preserve power relationships. Thus the constants r and q are required to satisfy

$$2r + 2q = r - 1. \tag{20}$$

The governing equation becomes

$$\left[\frac{GG''}{m} + G'^2\right] - a\left[rG + q\eta G'\right] = 0. \tag{21}$$

and we look for a solution of the form

$$G = c_1 + c_2\eta + c_3\eta^2 \tag{22}$$

noting that there may be other solutions to (21) that are not of the form of (22). From the boundary conditions listed in (17), the solution to (22) is determined to be

$$G = 1 - \eta^2. \tag{23}$$

The reader may check that the solution shown in (23) also satisfies (17b), as required. Substituting (23) into (21),

$$\frac{-2}{m}(1-\eta^2) + 4\eta^2 - a\left(r + \eta^2\right)(-r - 2q) = 0 \tag{24a}$$

and, from (20),

$$\frac{-2}{m}(1-\eta^2) + 4\eta^2 - a\left[r + \eta^2\right] = 0. \tag{24b}$$

We now wish to solve for the three unknown constants (a, r, q). All three constants appear in the similarity construct and can be related explicitly to m, the only parameter of the transformed differential equation (11). By equating coefficients of powers of η in (24b), we obtain two conditions for the constants r and a, required for a solution of the governing equation (21):

Equating coefficients of η^2

$$\frac{2}{m} + 4 - a = 0. \tag{25a}$$

Equating coefficients of η^0

$$\frac{-2}{m} - ar = 0. \tag{25b}$$

With (20), we have three equations for three unknowns (a, r, q). The result is

$$a = 2(1+2m)/m \tag{26a}$$

$$r = -1/(1+2m) \tag{26b}$$

$$q = -m/(1+2m). \tag{26c}$$

This completes the solution of the problem in the sense that all constants required by the similarity construct are given in terms of the parameter m, and once some form of $\alpha(x)$ has been chosen, (13), (15), (16), and (23) can be used to relate the integral in (12) back to the h variable. The solution is

$$h(x,y) = \alpha^{-1/m}\left(1 + a\int_0^x \frac{dx'}{\alpha^{1/m}}\right)^r\left[1 - y^2\left(1 + a\int_0^x \frac{dx'}{\alpha^{1/m}}\right)^{2q}\right] \tag{27}$$

where a, r, and q are given in terms of m in (26) and $\alpha = \alpha(x)$ is arbitrary. We note that for Newtonian fluids (m=3), our solution reduces to *Smith*'s [1973] solution, with a=14/3, r=-1/7 and q=-3/7.

Recall that the variables in (27) are dimensionless; they were nondimensionalized according to the transformations of (7). Here, we undo those transformations, arriving at

$$\left(1 + a\alpha_0^{1/m}\int_0^{x/L} \frac{dx'}{\alpha^{1/m}}\right)^r\left[1 - \frac{y^2}{w_0^2}\left(1 + a\alpha_0^{1/m}\int_0^{x/L} \frac{dx'}{\alpha^{1/m}}\right)^{2q}\right]. \tag{28}$$

The explicit form of $w(x)$ naturally follows from (6c) and (28). At the flow margin (i.e., $y = \pm w$),

$$1 - \frac{y^2}{w_0^2}\left(1 + a\alpha_0^{1/m}\int_0^{x/L} \frac{dx'}{\alpha^{1/m}}\right)^{2q} = 0 \tag{29a}$$

therefore

$$w = w_0\left(1 + a\alpha_0^{1/m}\int_0^{x/L} \frac{dx'}{\alpha^{1/m}}\right)^{-q}. \tag{29b}$$

Effect of Rheology on the Steady State Similarity Solution

The steady state similarity solution $h(x,y)$ (equation (28)) has a rheological dependence; both $\alpha(x)$ and m are prescribed

by the rheology of the fluid. We note, with the conditions given in (6), that regardless of the values of $\alpha(x)$ and m, (28) reduces to

$$h(0,y)=h_0\left(1-y^2/w_0^2\right). \tag{30}$$

The similarity method produces a physically realistic boundary condition: equation (30) indicates a parabolic cross section at the vent. The downstream evolution of this parabolic form, however, varies with the rheological characteristics. Here, we show the effect of various values of $\alpha(x)$ and m on the form of $h(x,y)$ both in cross-sectional and longitudinal profiles. In the following section, we compare the resulting profiles with data obtained from field and photographic measurements.

Models for $\alpha(x)$

During surface flow, a lava (or other geologic material) often experiences a change in resistance to flow. This could be due to changes in the fluid's properties (e.g., a downstream increase in viscosity in a lava due to cooling or crystallization) and/or changes in the underlying topography (e.g., changes in the slope or roughness of the underlying flow bed). Determining the nature of these processes and their effect on $\alpha(x)$ requires either empirical data from specific applications or an independent physical law, such as a cooling-induced viscosity or crystallinity change. In the absence of such information, we consider three end-member models to approximate the form of changes in $\alpha(x)$ with distance from the source of the flow. These choices of $\alpha(x)$ are arbitrary, but based on our knowledge that at least for Newtonian flows, $\alpha(x)$ is inversely related to viscosity. Here, we assume that $\alpha(x)$ is inversely related to viscosity in the general, non-Newtonian case and construct three models for $\alpha(x)$ correspond to constant, linearly increasing and exponentially increasing viscosity:

Constant $$\alpha(x)=\alpha_0 \tag{31a}$$

Linear $$\alpha(x)=\alpha_0/(1+x/L_\alpha) \tag{31b}$$

Exponential $$\alpha(x)=\alpha_0 e^{-x/L_\alpha} \tag{31c}$$

where $\alpha_0=\alpha(0)$ and L_α is a constant scale factor. For laminar flow of Newtonian fluids, $\alpha_0=1/3\nu_0$, where ν_0 is the viscosity at the source of the flow. Equation (31a) precludes any downstream changes in viscosity, thus requiring α to remain constant. Equations (31b) and (31c) allow for downstream viscosity changes. In formulating these two equations, we assumed viscosity increases downstream. For many geological materials (including silicate lava flows), this is consistent with observations that cooling and crystallization induce viscosity increases. However, this is not always the case; some materials (e.g., sulfur) show a decrease in viscosity during cooling in certain temperature ranges, and the reader is hereby cautioned. The rate at which viscosity increases (and $\alpha(x)$ decreases) in (31b) and (31c) is related to some scale factor L_α, which is generally controlled by physical processes (e.g., crystallization) and may be unrelated to the length scale L defined in (7b).

Effect of Rheology on the Solution

In this section we substitute the expressions for $\alpha(x)$ given in (31) into our solution for flow depth (equation (28)) and half width (equation (29b)) along with selected m values to determine the dependence of our solution on these rheological parameters. We note that the purpose of these calculations is to examine flow behavior for various flow regimes and not to model a realistic flow. Also required by these equations are flow depth and half width at the source (h_0 and w_0) and surface slope θ. Arbitrarily chosen sample values used in this analysis are given here: w_0=10 m, h_0=1 m and θ=5.7°. Substituting these parameters into (28) and (29b) allows us to construct depth and width profiles, respectively, for choices of $\alpha(x)$ and m and thus to determine the effect of these rheological parameters on our solution. Longitudinal depth and width profiles are shown for selected

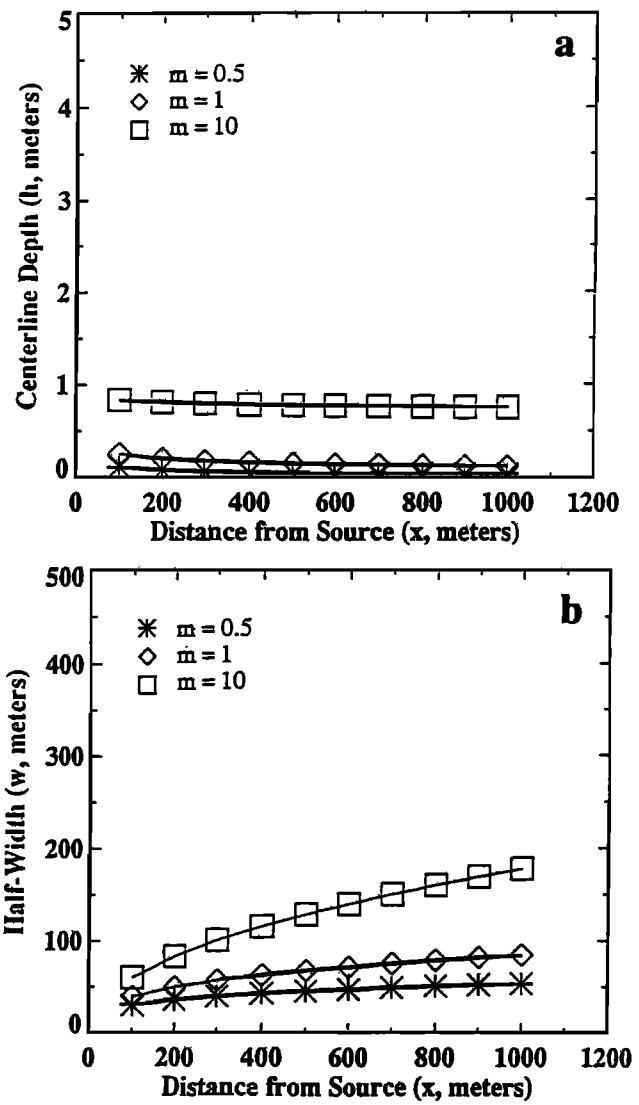

Figure 1. Theoretical longitudinal profiles of (a) centerline flow depth and (b) flow half width as a function of distance from source, based on constant viscosity and assumed initial parameters. These profiles correspond to m=0.5, m=1, and m=10. All flows (regardless of m values) widen downstream, accompanied by modest thinning. Higher m values correspond to wider, thicker flows having higher aspect ratios.

m values (0.5, 1, and 10) for constant (Figure 1), linearly increasing (Figure 2) and exponentially increasing viscosity (Figure 3).

For constant α, all flows (regardless of *m* values) widen downstream (Figure 1). Flow depth remains relatively constant, showing a slight downstream thinning. Higher *m* values correlate with wider, thicker flows of higher aspect ratios (*h*/*w*). Near the source, the flow has the highest aspect ratio; cross-sectional profiles become progressively thinner and wider downstream. All flows show convex longitudinal depth (*h* versus *x*) profiles (Figure 1a) and concave longitudinal width (*w* versus *x*) profiles (Figure 1b).

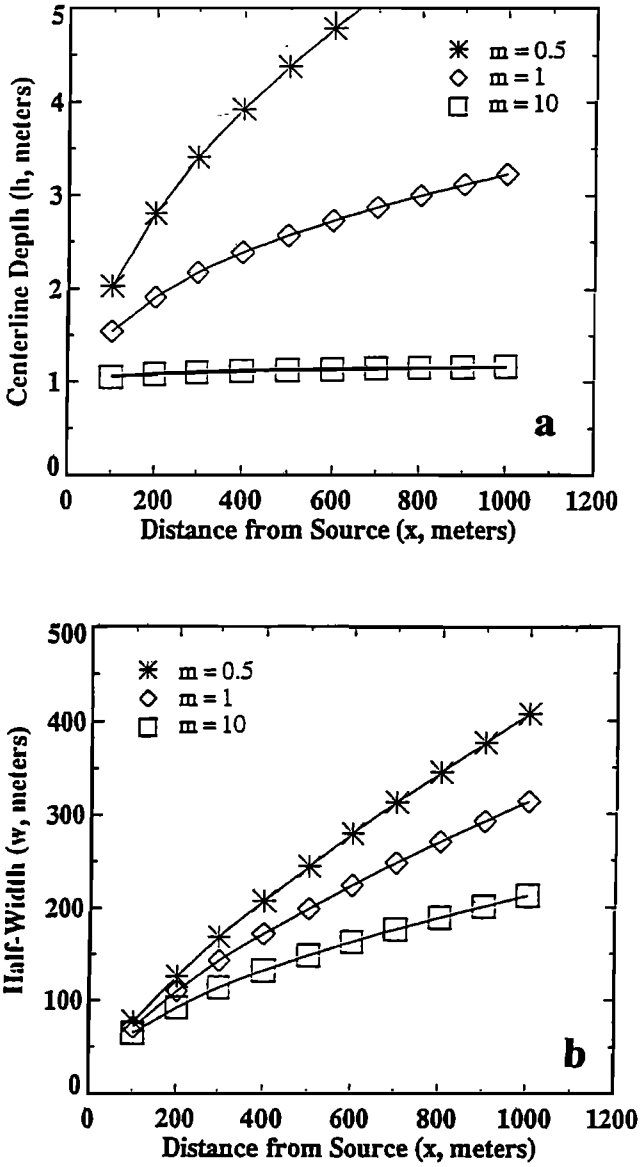

Figure 2. Theoretical longitudinal profiles of (a) centerline flow depth and (b) flow half width as a function of distance from source, based on linearly increasing viscosity and assumed initial parameters including L_α=10 (100-fold viscosity increase). These profiles correspond to *m*=0.5, *m*=1, and *m*=10. All flows (regardless of *m* values) thicken and widen downstream. Lower *m* values generally correlate with wider, thicker flows having higher aspect ratios.

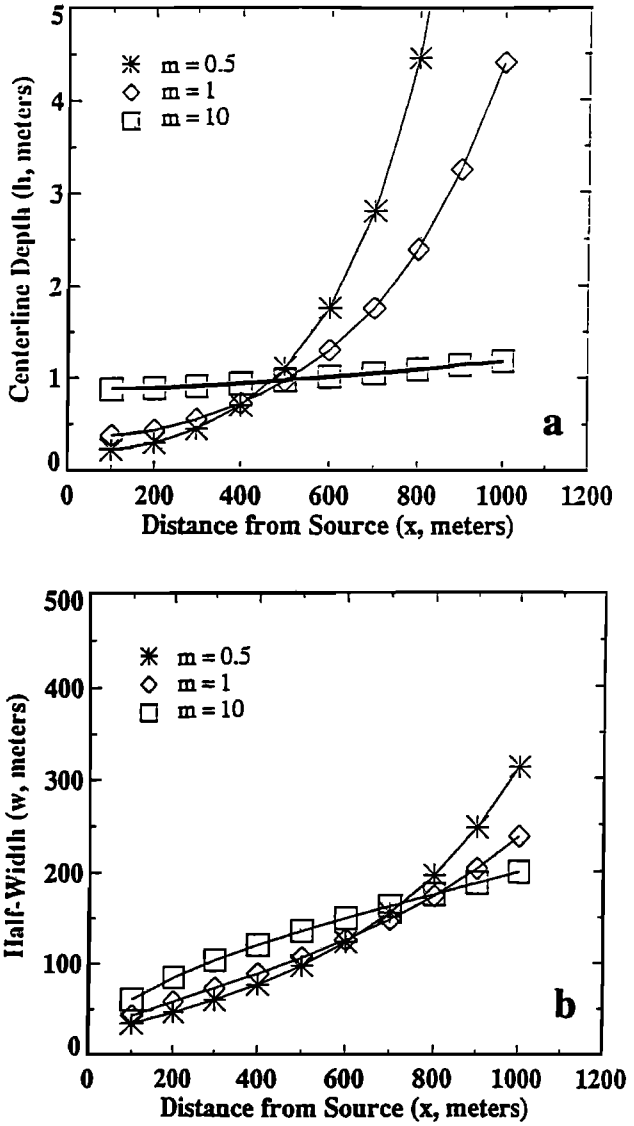

Figure 3. Theoretical longitudinal profiles of (a) centerline flow depth and (b) flow half width as a function of distance from source, based on exponentially increasing viscosity, and assumed initial parameters including L_α=215 (100-fold viscosity increase). These profiles correspond to *m*=0.5, *m*=1, and *m*=10. All flows (regardless of *m* values) thicken and widen downstream, but flows characterized by low *m* values show only modest widening and thickening over the distance shown (1 km).

For linear α (i.e., linearly increasing viscosity), flows tend to thicken and widen downstream. Unlike the case of constant α, lower *m* values generally correlate with wider, thicker flows having higher aspect ratios (Figure 2). Both the longitudinal depth (Figure 2a) and width (Figure 2b) profiles are concave. Compared with the case of constant α, these flows are wider and thicker, with the differences becoming more pronounced downstream, that is, as the differences in α(*x*) become more significant.

There is a strong dependence on the choice of scaling factor L_α. For sufficiently large values of L_α, downstream increases in α(*x*) are negligible, approximating constant viscosity. Thus the flow would exhibit a near-constant, slowly decreasing depth in a convex longitudinal depth

profile. Choosing sufficiently small L_α, the downstream longitudinal profile would show continuous thickening, most noticeably for low m values. Figure 2 is based on L_α=10 in (31b), which corresponds to a downstream viscosity increase of 100-fold over the first kilometer. This downstream viscosity increase is realistic for basaltic lavas, as discussed below.

For exponential α (i.e., exponentially increasing viscosity), flows tend to thicken and widen downstream. Like Figure 2, Figure 3 corresponds to a viscosity increase of 2 orders of magnitude over the first kilometer. This corresponds to L_α=215 in (31c). Flow depth (Figure 3a) and width (Figure 3b) each increase exponentially downstream. Longitudinal depth profiles are convex, whereas the width profiles may show a change in concavity from concave near the source to convex farther downstream. Flows characterized by low m values show only modest widening and thickening near the source; however, farther downstream, these flows eventually become thicker and wider than those characterized by higher m values. Again, there is a strong dependence on the choice of L_α. Choosing a smaller value for L_α would result in significantly wider and thicker longitudinal profiles.

Our model predicts that flows characterized by downstream viscosity increases (either linear or exponential) are typically thicker and wider than those flows that show no such viscosity increases (Figures 1-3). This is reasonable, consistent with observations that lava flows tend to "pile up" as they cool. Both the linear and exponential viscosity models predict downstream widening and thickening. Since the model assumes volume conservation, such concomitant widening and thickening necessarily implies a decrease in flow rate.

Comparison of Data and Theory

By comparing the theoretical profiles predicted by the model with known flow dimensions, we can work "backward" to infer the rheology of geologic deposits. This can be a valuable method of studying lavas whose flow has not been recorded, including prehistoric flows and flows in remote areas on Earth or other planets. However, we note that this model is simplified and must be applied with caution. One key assumption is flow must be unconfined. Once a channel and/or levees have been formed, flow becomes confined and tends to maintain an equilibrium width. Furthermore, the underlying topography is assumed to be smooth and characterized by constant slope. It is essential that this condition be satisfied because a lava of constant viscosity flowing on irregular topography may form a deposit having dimensions similar to that of a lava flowing on a smooth surface that cools during flow. Finally, our model assumes downstream flow is driven by gravitational transport, as opposed to being driven by hydrostatic pressure. If these assumptions are satisfied by a given flow, matching the flow's geometric dimensions to those predicted by the model can be used to infer or constrain the governing rheology (i.e., the rheological parameters $\alpha=\alpha(x)$ and m). A quantitative comparison between such theoretical and actual profiles is the focus of this section. However, this comparison is restricted to width profiles: without a priori knowledge of preexisting topography, centerline depth profiles cannot be accurately constructed.

Data

The database for this analysis consists of eight basaltic lava flows (or segments thereof). Each flow included in this study is an individual flow unit, as compound flows or flow fields are not described by our model. In choosing suitable candidates for measurement, we used the following criteria: (1) unconfined, gravity-driven flow; (2) continuous, well-preserved and unobscured flow margin; (3) constant surface slope; and (4) relatively smooth substrate such that any irregularities in the substrate do not significantly affect flow behavior. Five of the eight lava flows analyzed are tholeiite basalts on Kilauea volcano that were observed directly in the field. These flows are individual pahoehoe toes, with lengths ranging from 0.6 to 5 m from the point of breakout. Three of these pahoehoe toes have ropy morphology; the remaining two are smooth-surfaced. We measured flow width as a function of distance from the source. For two ropy pahoehoe flows, we also constructed an additional longitudinal width profile: we measured the end-to-end widths of the ropes at various downstream locations. No such measurement could be made on the third ropy toe, as it had a double-rope morphology.

We also constructed longitudinal profiles of flow width of three basaltic lavas from remote sensing images: La Poruña (Andes, Chile), Marcath flow (Lunar Crater, United States) and SP flow (San Francisco Volcanic Field, United States); see Figure 4. Each of these lavas met the suitability criteria outlined above. These flows range in composition from alkali basalt to basaltic andesite and are several kilometers in length [*Schaber et al.*, 1980; *Lum et al.*, 1989, *Francis*, 1993].

Methodology

In this paper, we compare the model's theoretical profiles of flow width against measurements obtained from our field and photographic studies. To generate these profiles, the model requires a variety of input parameters. Some of these parameters (i.e., h_0 and θ) are easily measured; others (i.e., m and α) are unknown and must be deduced. Recall that m is characteristic of the fluid so its value remains constant during flow (e.g., Newtonian fluids have m=3), whereas the parameter α records changes in viscosity during flow. Our model assumes any cross-stream variations in α are negligible, that is, $\alpha=\alpha(x)$. We consider three end-member approximations for $\alpha(x)$, all based on the assumption that α is inversely related to viscosity. These three models for $\alpha(x)$, corresponding to constant, linearly increasing, and exponentially increasing viscosity, are given in (31). Note that our solution for flow depth (equation (28)) and half width (equation (29b)) is not sensitive to absolute values of α_0, only to the ratio of $\alpha_0/\alpha(x)$. Thus α_0 is a free parameter which we define as α_0=1. In all cases, we assume a point source (i.e., w_0=1).

Our approach is to first consider only the field data. These flows are sufficiently short (< 5 m) such that viscosity (and thus α) is assumed constant. Thus the only unknown input parameter is m, which can be deduced by a best fit of the model to the data. We assume this value of m to be characteristic of all basaltic lavas.

We then consider the remote sensing data. Over the length of these flows (2-8 km), significant cooling and/or crystallization may have occurred, resulting in a downstream

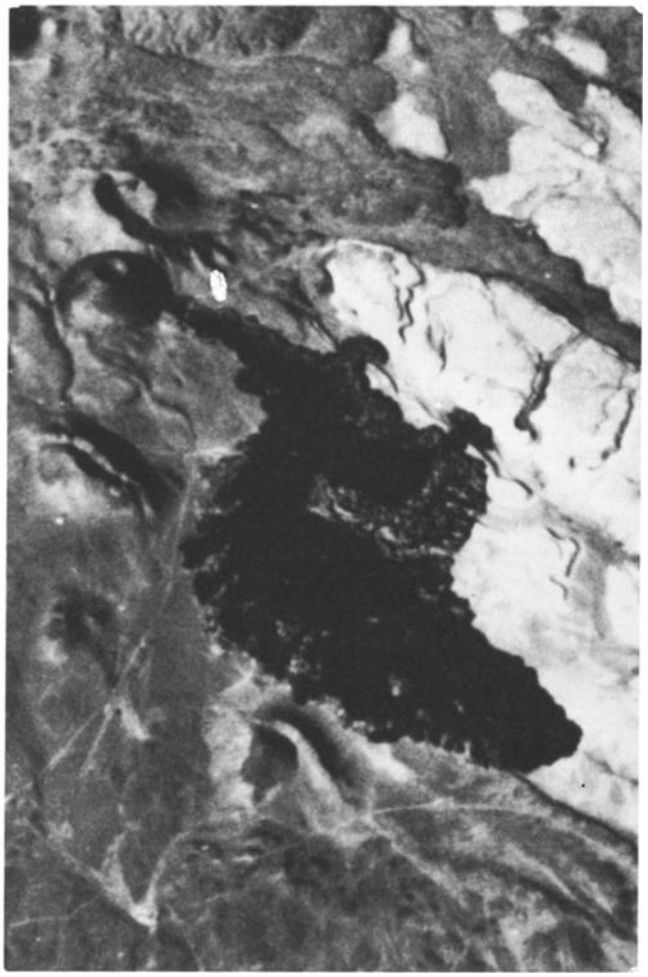

Figure 4a. Image of SP flow, located in the San Francisco Volcanic Field, United States. The flows in Figures 4a-4c are all basaltic and were selected according to the criteria described in the text.

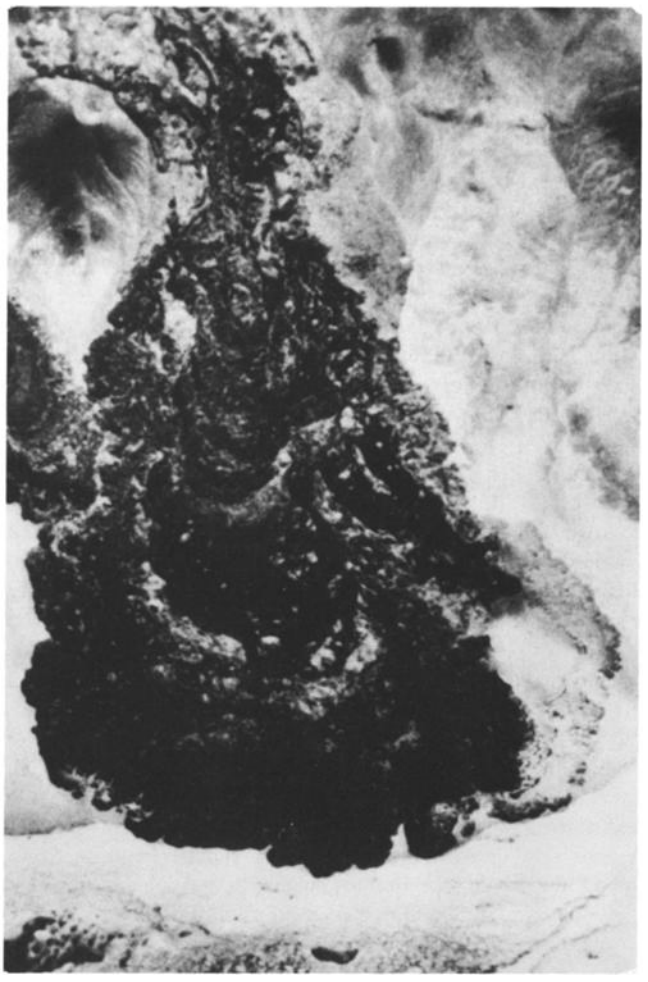

Figure 4b. Image of Marcath flow, Lunar Crater, United States.

Figure 4c. Image of La Poruña flow, located in the Andes Mountains in northern Chile.

viscosity increase. Thus we cannot assume constant α. However, using the m value obtained from the field data above, the form of $\alpha(x)$ can be inferred for each flow by fitting the model to these data. By computing the corresponding predicted viscosity increase, the model can be tested for reasonableness.

Results: Field Data

In accordance with the above described methodology, we begin our analysis by comparing the field data with the theoretical output of our fluid dynamic model assuming constant viscosity. For the majority of the field data, the best fit of the model is obtained using m values of 1-2 (Figure 5). (We note, however, the data do not all appear concave as predicted by the constant-viscosity model.) We assume this value of m to be characteristic of all basaltic lavas.

As Newtonian fluids are characterized by m=3, our analysis suggests most basaltic flows are non-Newtonian.

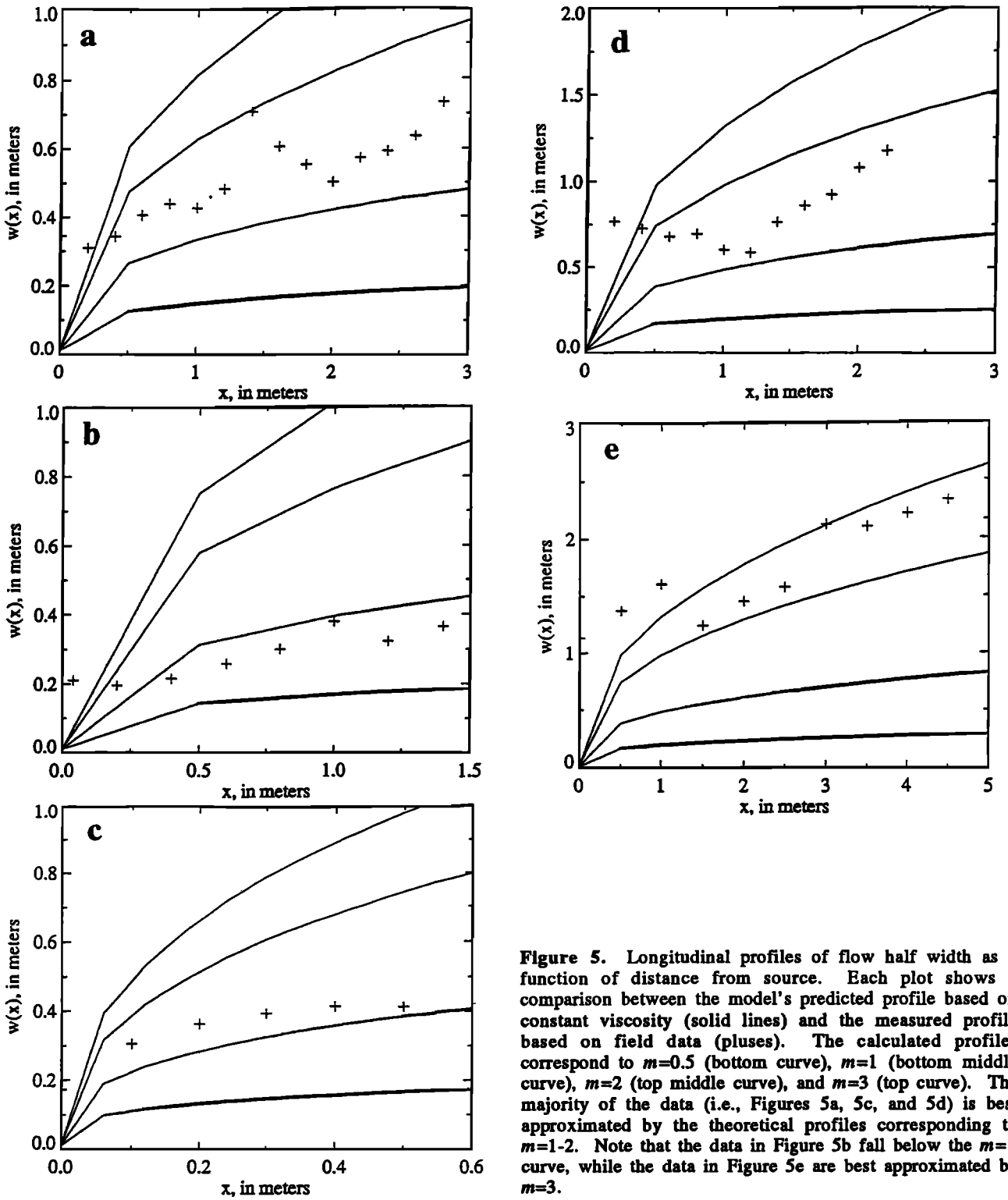

Figure 5. Longitudinal profiles of flow half width as a function of distance from source. Each plot shows a comparison between the model's predicted profile based on constant viscosity (solid lines) and the measured profile based on field data (pluses). The calculated profiles correspond to m=0.5 (bottom curve), m=1 (bottom middle curve), m=2 (top middle curve), and m=3 (top curve). The majority of the data (i.e., Figures 5a, 5c, and 5d) is best approximated by the theoretical profiles corresponding to m=1-2. Note that the data in Figure 5b fall below the m=1 curve, while the data in Figure 5e are best approximated by m=3.

Equation (4) predicts these basaltic flows, with their lower m values, to be thicker than Newtonian flows emplaced at the same flow rate. This is in agreement with a wide variety of field and laboratory measurements of basaltic lavas which indicate the presence of a yield strength [e.g., *Shaw et al.*, 1968; *Shaw*, 1969; *Pinkerton and Sparks*, 1978]. This non-Newtonian rheology has been attributed to dispersed crystals and gas bubbles contained in the lava and possibly to the development of molecular structural units at subliquidus temperatures (as summarized by *Cas and Wright* [1987, section 2.4]).

As discussed above, we also measured the widths of surface ropes as a function of downstream location of two pahoehoe flows. (Rope width is defined as the linear distance between the endpoints of each rope.) These data are shown along with the model's predicted longitudinal width profiles for various m (Figure 6). For both flows, the model approximates the data for $1/2 < m < 1$. Recall that our model assumes unconfined flow. We conducted these rope width measurements because we were interested in seeing how our model would fit data of confined flow. Like the flow itself, the ropes widen downstream. However, the downstream widening of the ropes is hampered by the confining effect of the previously established flow margins. Thus we might expect the ropes to experience less net widening compared to the total flow, corresponding to a smaller m value. This is precisely what Figure 6 shows.

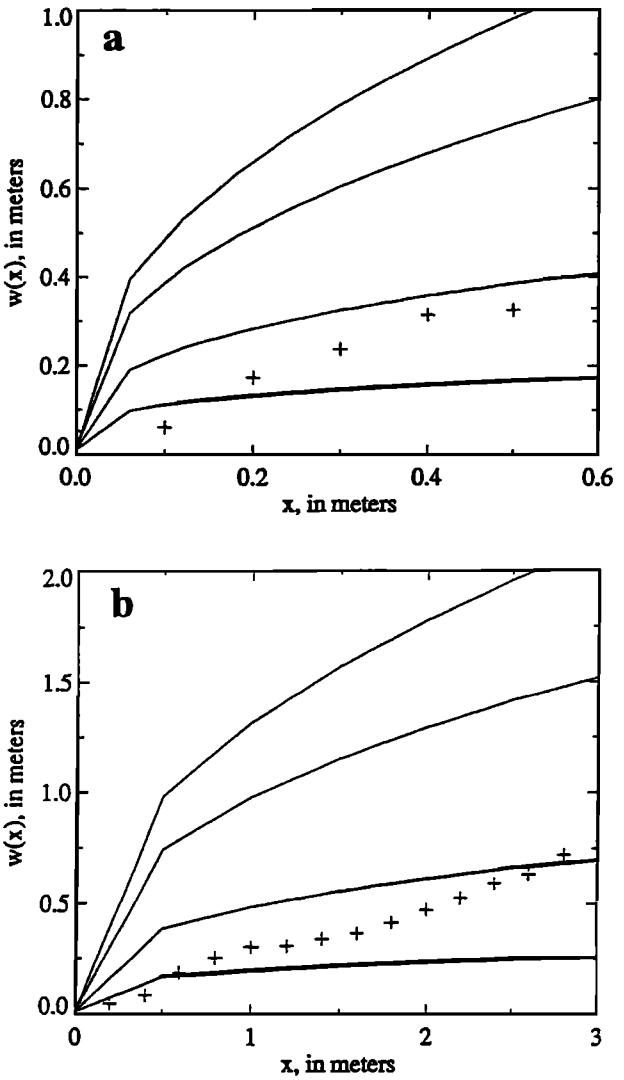

Figure 6. Longitudinal profiles of rope half width as a function of distance from source. Each plot shows a comparison between the model's predicted profile based on constant viscosity (solid lines) and the measured profile based on field data (pluses). The calculated profiles correspond to m=0.5 (bottom curve), m=1 (bottom middle curve), m=2 (top middle curve), and m=3 (top curve). These data are best approximated by the theoretical profiles corresponding to m=0.5-1.

Results: Remote Sensing Data

Using m values of 1 and 2, we run the model for parameters corresponding to the remote sensing data, based on the assumption of constant viscosity. Figure 7 shows the resulting longitudinal width profiles. For all flows, the data are inconsistent with the model's predictions. The measured widths generally exceed those predicted by the model, and these differences become more pronounced downstream. This results in a steeper longitudinal width profile than that predicted by the model. The inconsistency between these data and the model's predictions suggests that basaltic flows of these lengths are generally characterized by a downstream viscosity increase.

Using the same m values and initial parameters, we rerun the model based on the assumption of nonconstant viscosity. Figures 8 and 9 show longitudinal width profiles for linearly and exponentially increasing viscosities, based on (31b) and (31c), respectively. In these equations, the parameter L_α quantifies the downstream viscosity increase. In the absence of actual data or an empirical law, a value of L_α must be assumed. Choosing L_α sufficiently large has the effect of reducing (31b) and (31c) to (31a), the case of constant viscosity. In this work, our method is to first chose a value of L_α empirically to approximate the data and then to test this value for reasonableness by calculating the corresponding change in viscosity. This approach results in choices of L_α=50 (Figure 8) and L_α=500 (Figure 9).

Compared to the constant viscosity model, the linear viscosity model more closely approximates the data for all three flows (Figure 8). For two of these flows (Lunar Crater and SP), the exponential viscosity model also produces a good fit to the data (see Figures 9a and 9b). The downstream viscosity increases corresponding to the model predictions shown in Figures 8 and 9 are 2 and 3-4 orders of magnitude, respectively, over a distance of 4 km. These downstream viscosity increases are comparable to those documented for basaltic flows; see *Crisp et al.* [1994] for a review of the literature. The viscosity of the 1983-1984 Pu'u O'o flows has been measured by *Fink and Zimbelman* [1990] to have increased approximately 2 or 3 orders of magnitude during emplacement. *Moore and Ackerman* [1989] similarly estimate downstream viscosity increases of Kilauea basalts to be 2 orders of magnitude. For basaltic flows from Mount Etna, *Booth and Self* [1973] estimate viscosity increases of 2 orders of magnitude over 4 km. Thus the downstream viscosity increases corresponding to the linear and exponential viscosity profiles shown in Figures 8 and 9 are reasonable.

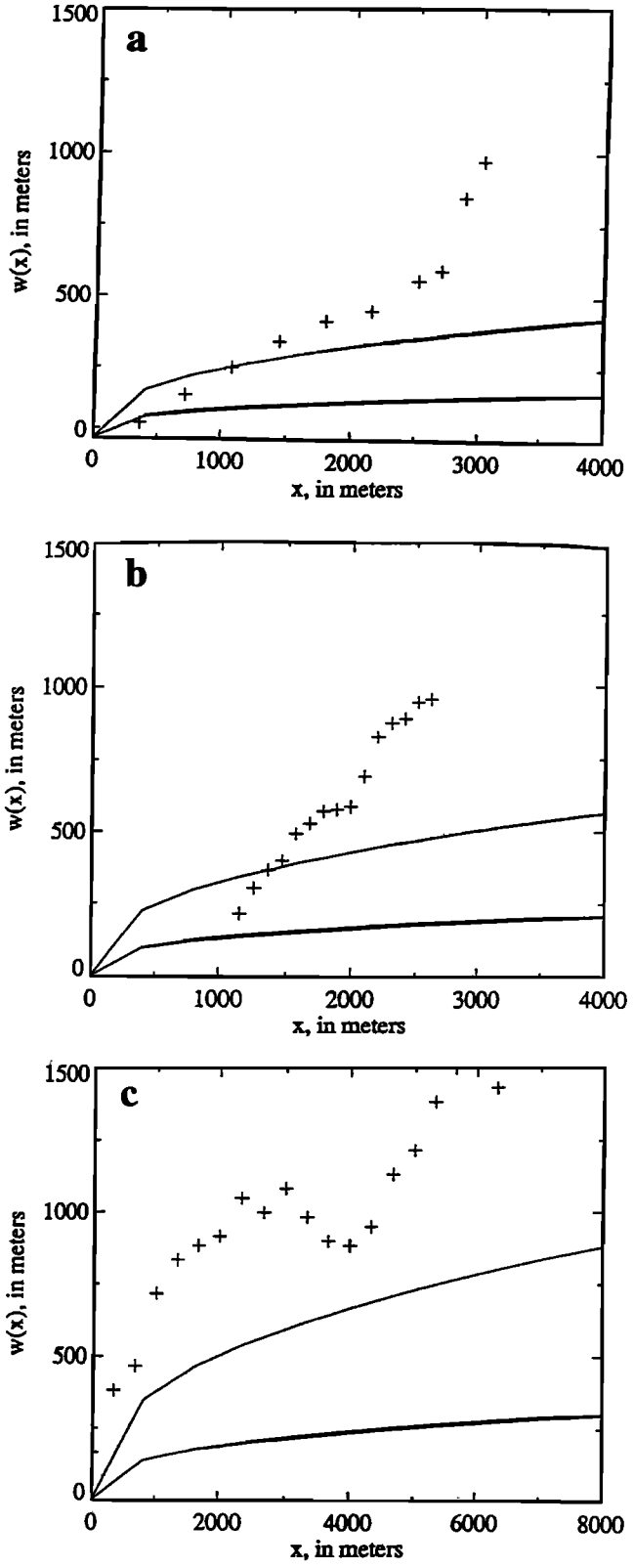

Figure 7. Longitudinal profiles of flow half width as a function of distance from source. Each plot shows a comparison between the model's predicted profile based on constant viscosity (solid lines) and the measured profile based on remote sensing data (pluses). The calculated profiles correspond to m=1 (bottom curve) and m=2 (top curve). Remote sensing data are of (a) SP flow, (b) Marcath Flow, Lunar Crater, and (c) La Poruña flow. In all cases, the data are steeper than the given theoretical profiles based on constant viscosity.

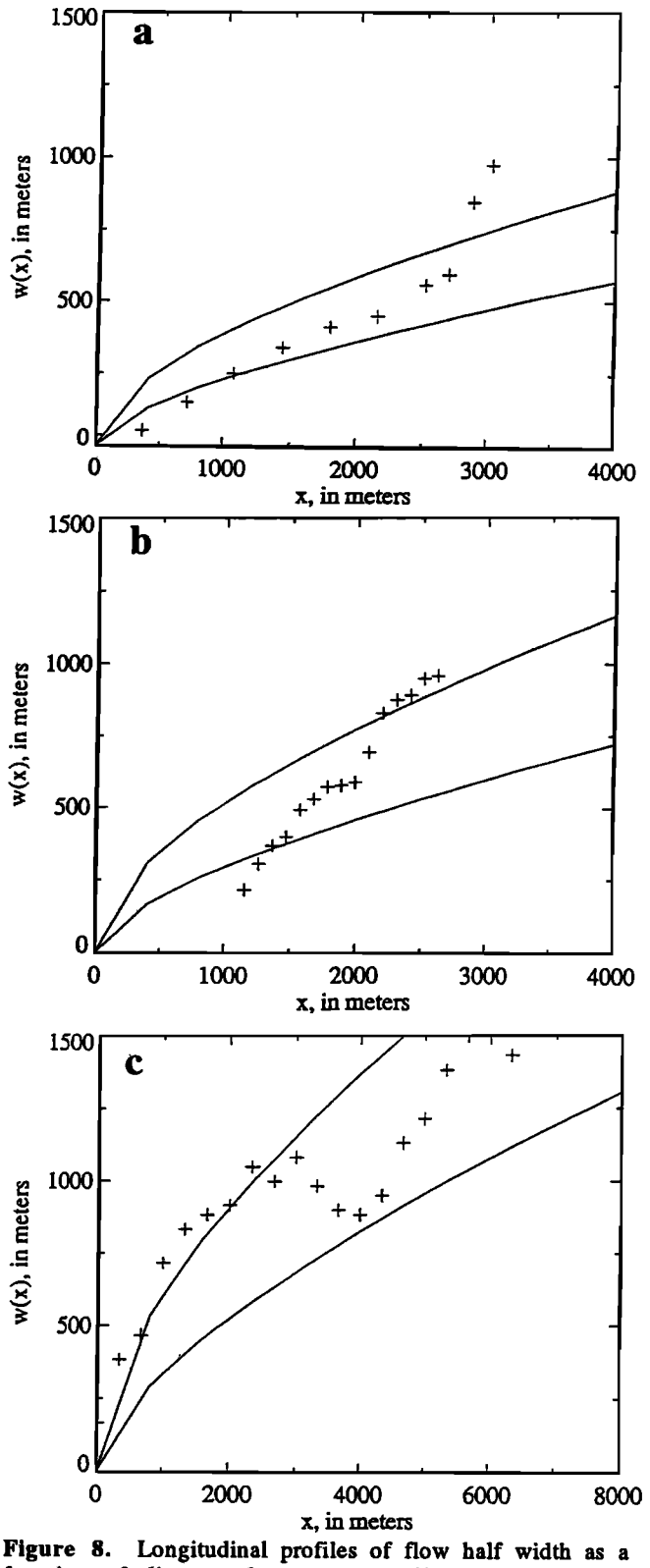

Figure 8. Longitudinal profiles of flow half width as a function of distance from source. Each plot shows a comparison between the model's predicted profile based on linear viscosity (solid lines) and the measured profile based on remote sensing data (pluses). The calculated profiles correspond to m=1 (bottom curve) and m=2 (top curve). For both profiles, L_α=50, which corresponds to a downstream viscosity increase of ~2 orders of magnitude over 4 km. Remote sensing data are of (a) SP flow, (b) Marcath Flow, Lunar Crater, and (c) La Poruña flow. Data of all three flows are better approximated by this linear viscosity model than the constant viscosity model shown in Figure 7.

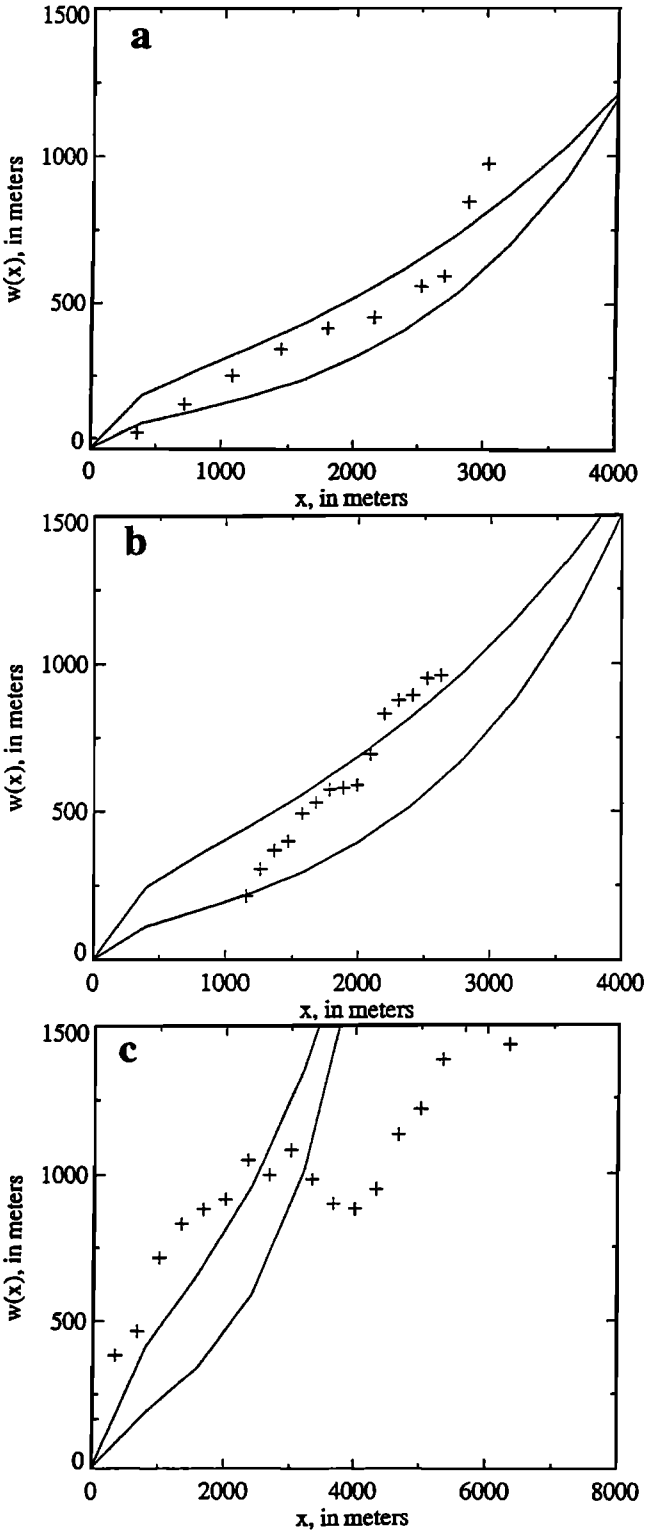

Figure 9. Longitudinal profiles of flow half width as a function of distance from source. Each plot shows a comparison between the model's predicted profile based on exponential viscosity (solid lines) and the measured profile based on remote sensing data (pluses). The calculated profiles correspond to m=1 (bottom curve) and m=2 (top curve). For both profiles, L_α=500, which corresponds to a downstream viscosity increase of 3-4 orders of magnitude over 4 km. Remote sensing data are of (a) SP flow, (b) Marcath Flow, Lunar Crater, and (c) La Poruña flow. The data in Figures 9a and 9b are better approximated by this exponential viscosity model than the constant viscosity model shown in Figure 7.

Conclusions

Steady State Similarity Solution

Using a similarity transformation, we found an exact analytic solution in the steady state for gravity-driven flows on an inclined plane. In formulating the governing equation, we assumed that volume is conserved and that the magmastatic pressure gradient in the downstream direction is small relative to the influence of gravity. Our solution predicts downstream changes in flow depth and width for different rheological characteristics based on known or assumed initial parameters.

Non-Newtonian Rheology

Figure 5 shows a comparison of longitudinal width profiles of sample field data and model predictions, assuming constant viscosity. The majority of these field data are well approximated by the constant viscosity model, for m between 1 and 2. This indicates non-Newtonian rheology, as Newtonian fluids are characterized by m=3. This is in agreement with numerous field and laboratory studies of basaltic lavas which indicate the presence of a yield strength [e.g., *Shaw et al.*, 1968; *Shaw*, 1969; *Pinkerton and Sparks*, 1978]. Physically, the relatively low m values of these basaltic flows indicate relatively thin flows, compared with Newtonian flows emplaced at the same flow rate.

Downstream Viscosity Increases

Using m values of 1 and 2, we ran the model for three end-member approximations of α: corresponding to constant, linearly increasing and exponentially increasing viscosity. The remote sensing data are inconsistent with the model's predictions for constant viscosity (constant α). Instead, they are better approximated by linear or exponential models corresponding to downstream viscosity increases of 2-4 orders of magnitude, over a distance of 4 km. The reasonableness of these values attests to the validity of this model.

Notation

q	volumetric flow rate per unit width.
x	spatial coordinate in the downstream direction (parallel to slope).
y	spatial coordinate in the cross-stream direction (perpendicular to slope).
z	spatial coordinate related to x, defined in equation (13).
t	time.
α	a spatially dependent, empirically determined rheological parameter.
α_0	α at the source.
h	flow depth.
h_0	flow depth at the source.
w	flow half width.
w_0	flow half width at the source.
b	an empirically determined constant.
m	an empirically determined positive constant.
g	gravitational acceleration.
ν	kinematic viscosity.
θ	slope.
$f(\theta)$	some function of slope.

L	characteristic length scale.
L_α	scaling factor for α.
a, r, q	constants of similarity construct, defined in terms of m in equation (26).
ξ, G, η	variables of similarity construct, defined in equations (15) and (16).

Acknowledgments. This research was funded by NASA grants NGT 50930 and NAGW 3684. We thank L. Glaze, D.F. McTigue, G. Weir and an anonymous reviewer for their thoughtful reviews. This manuscript also benefited from useful discussions with D. Bercovici and X. Tata (University of Hawaii) and S. Blake (The Open University). Images were provided by R. Lopes-Gautier (Jet Propulsion Laboratory, NASA) and P. Francis (The Open University). Many thanks to University of Hawaii staff M. Tatsumura (field assistance) and H. Garbeil (computer programming). This is SOEST contribution 4068 and HIGP paper 875.

References

Baloga, S., Lava flows as kinematic waves, *J. Geophys. Res.*, *92*, 9271-9279, 1987.

Booth, B., and S. Self, Rheological features of the 1971 Mount Etna lavas, *Philos. Trans. R. Soc. London A*, *274*, 99-106, 1973.

Bruno, B.C., G.J. Taylor, S.K. Rowland, P.G. Lucey, and S. Self, Lava flows are fractals, *Geophys. Res. Lett.*, *19*, 305-308, 1992.

Bruno, B.C., G.J. Taylor, S.K. Rowland, and S.M. Baloga, Quantifying the effect of rheology on lava-flow margins using fractal geometry, *Bull Volcanol.*, *56*, 193-206, 1994.

Cas, R.A.F., and J.V. Wright, *Volcanic Successions*, 528 pp., Allen and Unwin, Winchester, Mass., 1987.

Crisp, J., K.V. Cashman, J.A. Bonini, S.B. Hougen, and D.C. Pieri, Crystallization history of the 1984 Mauna Loa lava flow, *J. Geophys. Res.*, *99*, 7177-7198, 1994.

Fink, J.H., and J. Zimbelman, Longitudinal variations in rheological properties of lavas: Puu Oo basalt flows, Kilauea Volcano, Hawaii, in *Lava Flows and Domes. Emplacement Mechanisms and Hazard Implications*, edited by J.H. Fink, pp. 157-173, Springer-Verlag, New York, 1990.

Francis, P., *Volcanoes*, 443 pp., Oxford Univ. Press, New York, 1993.

Gol'din, B.M., and L.S. Lyubashevskiy, Computation of the velocity of mudflows in Crimean rivers, *Tr. Ukr. Nauchno Issled. Gidrometerol. Inst.*, *60*, 73-75, 1966.

Hunt, B., Asymptotic solution for dam-break problem, *J. Hydraul. Div. Am. Soc. Civ. Eng.*, *108*, 115-127, 1982.

Huppert, H.E., The propagation of two-dimensional and axisymmetric viscous gravity currents over a rigid horizontal surface, *J. Fluid Mech.*, *121*, 43-58, 1982a.

Huppert, H.E., Flow and instability of a viscous current down a slope, *Nature*, *300*, 427-429, 1982b.

Lighthill, M.J., and G.B. Whitham, On kinematic waves, I, Flood movement in long rivers, *Proc. R. Soc. London A*, *229*, 281-316, 1955.

Lister, J.R., Viscous flows down an inclined plane from point and line sources, *J. Fluid Mech.*, *242*, 631-653, 1992.

Lum, C.C.L., W.P. Leeman, K.A. Foland, J.A. Kargel, and J.G. Fitton, Isotopic variations in continental basaltic lavas as indicators of mantle heterogeneity: Examples from the western U.S. Cordillera, *J. Geophys. Res.*, *94*, 7871-7884, 1989.

Moore, H.J., and J.A. Ackerman, Martian and terrestrial lava flows (abstract), *Lunar Planet. Sci.*, *XX*, 711-712, 1989.

Nye, J.F., The response of glaciers and ice sheets to seasonal and climatic changes, *Proc. R. Soc. London A*, *256*, 559-584, 1960.

Nye, J.F., The response of a glacier to changes in the rate of nourishment and wastage, *Proc. R. Soc. London A*, *275*, 87-112, 1963.

Paterson, W.S.B., *The Physics of Glaciers*, 250 pp., Pergamon, Tarrytown, N.Y., 1969.

Pinkerton, H., and R.S.J. Sparks, Field measurements of the rheology of lava, *Nature*, *276*, 383-386, 1978.

Schaber, G.G., C. Elachi and T.G. Farr, Remote sensing data of SP mountain and SP lava flow in North-central Arizona, *Remote Sensing Environ.*, *9*, 149-170, 1980.

Shaw, H.R., Rheology of basalt in the melting range, *J. Petrol.*, *10*, 510-535, 1969.

Shaw, H.R., T.L. Wright, D.L. Peck and A.R. Okamura, The viscosity of basaltic magma: An analysis of field measurements in Makaopuhi lava lake, Hawaii, *Am. J. Sci.*, *266*, 225-264, 1968.

Sherman, B., Kinematic wave models for overland flow, *Appl. Math.*, *35*, 435-444, 1978.

Sherman, B., Channel flow with infiltration, *Appl. Math.*, *39*, 87-96, 1981.

Sherman, B., and V.P. Singh, A kinematic model for surface irrigation, *Water Resour. Res.*, *14*, 357-364, 1978.

Smith, P., A similarity solution for slow viscous flow down an inclined plane, *J. Fluid Mech.*, *58*, 275-288, 1973.

Weir, G.J., Kinematic wave theory for Ruapehu lahars, *N. Z. J. Sci.*, *25*, 197-203, 1982.

Weir, G.J., The asymptotic behaviour of simple kinematic waves of finite volume, *Proc. R. Soc. London A*, *387*, 459-467, 1983.

S. M. Baloga, Proxemy Research Inc., 20528 Farcroft Lane, Laytonsville, MD 20882.

B. C. Bruno, Department of Earth Sciences, The Open University, Walton Hall, Milton Keynes MK7 6AA, England. (e-mail: B.C.Bruno@open.ac.uk)

G. J. Taylor, Hawaii Institute of Geophysics and Planetology, University of Hawaii at Manoa, 2525 Correa Road, Honolulu, HI 96822. (e-mail: gjtaylor@kahana.pgd.hawaii.edu)

(Received August 10, 1995; revised December 21, 1995; accepted January 5, 1996.)